Swiss J Geosci (2011) 104:355–365
DOI 10.1007/s00015-011-0074-0

Tremolite–calcite veins in the footwall of the Simplon Fault, Antigorio Valley, Lepontine Alps (Italy)

Vito Meggiolaro · Michele Sapigni · Anna Maria Fioretti

Received: 23 February 2011 / Accepted: 19 August 2011 / Published online: 19 October 2011

Abstract The lowermost units of the nappe pile of the Lepontine Alps crop out in the Antigorio valley in the footwall of the Simplon Fault. The whole orthogneiss section of the Antigorio Unit is exposed on both sides of the valley, sandwiched between the Mesozoic metasedimentary sequences of the Baceno unit below and the Tèggiolo unit above. The petrography and mineral composition of tremolite–calcite veins occurring in dolomite marble in both metasedimentary sequences were investigated. Tremolite–calcite (with lesser talc and minor phlogopite) veins have rhythmic banded texture. Banding is due to cyclic differences in modal abundances and fabric of tremolite and calcite. These veins are very similar to those occurring in dolomite rafts within the Bergell granite and it is inferred that they formed by the same "fracture-reaction-seal" mechanism. Veins formed by reaction of a silica-rich aqueous fluid with the host dolomite marble along fractures. According to thermo-barometric calculations, based on electron microprobe analyses, reaction occurred at temperatures between 450 and 490°C and minimum pressure of 2–3 kbar. Such temperature conditions occurred in this footwall region of the Simplon Fault Zone around 15 Ma, during exhumation and cooling of the nappe pile and a transition to brittle behaviour. Aqueous, silica-rich fluids concentrated along fractures, forming tremolite–calcite veins in the dolomite marbles and quartz veins in the orthogneiss.

Keywords Tremolite · Vein · Simplon · Antigorio valley

Editorial handling: Edwin Gnos.

Electronic supplementary material The online version of this article (doi:10.1007/s00015-011-0074-0) contains supplementary material, which is available to authorized users.

V. Meggiolaro
Via Botticelli 3, Ponte San Nicolò, 35020 Padova, Italy

M. Sapigni (✉)
Engineering Department, ENEL SpA, Via Torino 16, 30172 Venezia-Mestre, Italy
e-mail: michele.sapigni@enel.com

A. M. Fioretti
CNR–Istituto Geoscienze e Georisorse, Unità Operativa di Padova, Via Gradenigo 6, 35131 Padova, Italy
e-mail: anna.fioretti@igg.cnr.it

1 Introduction

The Lepontine dome is one of the best studied areas of the central Penninic Alps, and its structural and metamorphic evolution, from the successive emplacement of the crystalline nappes, to their polyphase refolding and final exhumation in the footwall of the Simplon Fault Zone, is very well documented (Mancktelow 1985; Escher et al. 1993; Steck et al. 1999; Keller et al. 2005; Maxelon and Mancktelow 2005; Steck 2008). There is clear evidence that during final unroofing there was a diachronous passage from ductile to brittle deformation conditions in the footwall and hanging wall of the Simplon Fault Zone (Grasemann and Mancktelow 1993; Wawrzyniec et al. 1999; Zwingmann and Mancktelow 2004; Campani et al. 2010a, b).

This paper focuses on veins formed during the brittle phase of exhumation. One specific vein-type in metamorphic carbonates is represented by tremolite–calcite veins which develop in dolomite marbles. Some of these have been described in the metasedimentary cover of basement units in the Lepontine Alps (Mercolli et al. 1987) and in dolomite marble roof pendants in the Bergell intrusion (Bucher 1998). In this paper, we describe the mineralogical

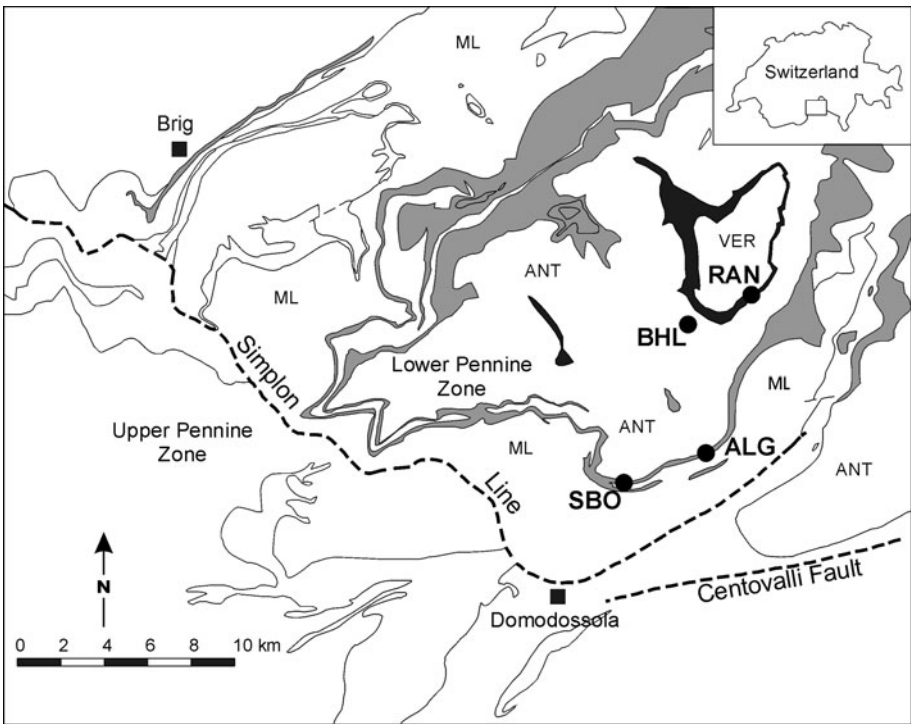

Fig. 1 Geological sketch of the area between the Verampio window and the Simplon Fault (modified after Grasemann and Mancktelow 1993 and Steck et al. 1999). Ortogneiss nappes: Verampio (VER), Antigorio (ANT), Monte Leone (ML). Mesozoic metasediments: Baceno (*black*), Tèggiolo (*grey*). Outcrop of Rio Antolina (RAN) and boreholes S4 and S8 (BHL) belong to Baceno metasediments. Outcrops of Simbo (SBO) and Alagua (ALG) belong to Tèggiolo metasediments. Swiss national grid coordinates of sampled veins: RAN 670340/120855; S4 667110/119005; S8 667130/118630; SBO 666225/112925; ALG 669590/116505

and petrographical characteristics of tremolite–calcite veins found in the western part of the Lepontine metamorphic dome in an area where regional metamorphism has not been affected by plutonism. We provide T–P constraints for the vein formation and propose a genetic model to explain the development of these late veins in relation to their position in the footwall of the Simplon low-angle normal fault.

2 Geological setting

The Lepontine dome consists of an Alpine stack of nappes made of pre-Triassic crystalline basement and intercalated Mesozoic metasediments (Steck 2008; Leu 1986). This structure reflects thrusting and folding produced by continental collision between the northern Tethyan margin and the Adriatic indenter (Steck 2008).

The lowermost part of the studied section consists of three major orthogneiss nappes (Verampio, Antigorio and Monte Leone) and two intercalated Mesozoic sequences (the Baceno and Tèggiolo metasediments; Fig. 1). Overthrusting of the crystalline basement nappes was lubricated by the weak Mesozoic sequences (Herwegh and Pfiffner 1999), as is the case for the basal thrust of the Antigorio nappe, where layers of gypsum and anhydrite have been recovered from recent boreholes (BHL S4 and S8 unpublished data) in the Crodo Area (Fig. 1). The main part of the two metasedimentary sequences is composed of calcite and dolomite marbles, with minor amounts of calc-schists, quarzites and phlogopitic-tremolitic calcite marbles (Castiglioni 1958; boreholes stratigraphy and detailed geological map, unpublished data).

In the present work we focus on tremolite–calcite veins recently found within the metasedimentary sequences. Veins exposed in the valley of Rio Antolina (RAN) and veins crosscut by boreholes S4 and S8 (BHL) belong to the Baceno metasediments cropping out in the centre of the Verampio window where the nappe pile is in a flat-lying setting. Veins exposed at Simbo (SBO) and Alagua (ALG) belong to the Tèggiolo metasediments. They are close to the Simplon Line in an area where the nappes are folded and steeply dipping SSE. In both areas no microstructural deformation feature of the Simplon Line is evident.

3 Previous works

The presence of tremolite in metasediments of the Lepontine Dome is known since the late 18th century, when Pini (1786) first described tremolite as a new mineral in the veins of the Triassic dolomite at Campolungo (Switzerland). Pioneering studies of Schardt (1903) and Schmidt and Preiswerk (1905) reported tremolite in metasediments of the Simplon region, and Cinque (1939) and Castiglioni (1958) described tremolite in the metasediments from our study area.

Within the mineral assemblages of metasediments from the Lepontine Dome tremolite is considered a valuable indicator of PT-conditions for metamorphic carbonates. Its first occurrence (tr-in) is used to define a mappable

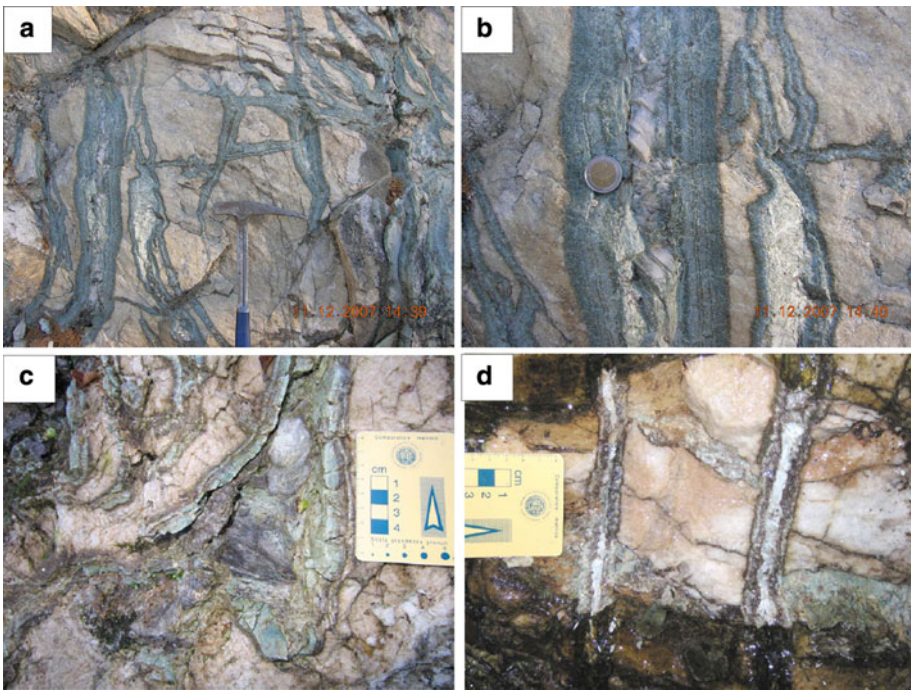

Fig. 2 General view of the stockwork of tremolite–calcite veins in Tèggiolo metasediments at Alagua (**a**, and close up view **b**) and veins in Baceno metasediments along Rio Antolina (**c**, **d**). Toward the tip, veins lack the core of calcite and part of the layered band. In **d** the inner part of the veins is made up only of *pale green* to *whitish* tremolite in needles and bundles of fibres slightly inclined with respect to the fracture wall. The two symmetrical outer layers are formed by needles of tremolite in a radial texture cemented by interstitial calcite and Fe–Mn oxides, the latter being responsible for the overall *brown colour*

metamorphic isograd (Trommsdorff 1966; Kuhn et al. 2005 and references therein). Tremolite veins of the Campolungo area formed around pre-existing quartz veins in dolomitic rocks due to the influx of aqueous fluids with a high salt contents (Bianconi 1971; Trommsdorff and Skippen 1986; Mercolli et al. 1987), reaching approx 5% in weight of NaCl-equivalent (Walther 1983).

Distinct tremolite veins are documented in the dolomitic limestone rafts within the Bergell intrusion (Bucher-Nurminen 1981; Bucher 1998). These veins formed by reaction of the dolomitic rock with silica-rich and NaCl-free hydrothermal fluids.

4 Petrography

Tremolite–calcite veins occur in massive dolomite marble where a very weak schistosity is defined by thin films of phlogopite. Veins are organised in a stockwork, with vein orientations not influenced by the orientation of the schistosity. Veins can represent up to 40% of the exposed volume and their thickness ranges from less than 1 cm to 20 cm (Fig. 2).

The veins display textural and compositional symmetric banding. Where complete (at Alagua and Rio Antolina), they consist of (from rims to centre; Fig. 3):

- a 1–3 mm thick brownish border that grades into the dolomitic marble;
- an outer band, up to 25 mm thick, made of one or several thin layers (3–5 mm), each mainly composed of green amphibole needles forming comb-like aggregates normal to the vein rims separated by calcite-rich layers;
- an inner band, up to 15 mm thick, of greenish-grey, centimetre long, needle-shaped tremolite crystals almost parallel to the vein rim;
- a 10–30 mm thick core composed of white to pale grey, very coarse calcite crystals.

Thinner veins may be incomplete and may lack the inner layers (Figs. 2d, 3). In all of the three investigated outcrops, tremolite occurs also in phlogopite calcite marble as 2–5 mm thick layers parallel to the schistosity, with tremolite contents ranging from 2 to 15% by volume.

A structural survey of the three outcrops showed that the veins formed along steep fracture sets with different orientations. The East–West trending direction is common to all the outcrops. Veins at Alagua (ALG) and Simbo (SBO) are dipping South, whereas at Rio Antolina (RAN) they are dipping North. Other important orientations of the fracture sets are NW–SE, dipping SW, and NE-SW, dipping NW. Other veins have random orientations, which give the rock mass the overall stockwork structure. Since the main fracture set has a similar orientation in the different outcrops, it is likely that the veins formed after the regional folding.

4.1 Microscopic description

The host rock of the tremolite–calcite veins is a granoblastic, homeoblastic, fine grained (0.4–0.8 mm) dolomite marble with straight grain boundaries and triple junctions

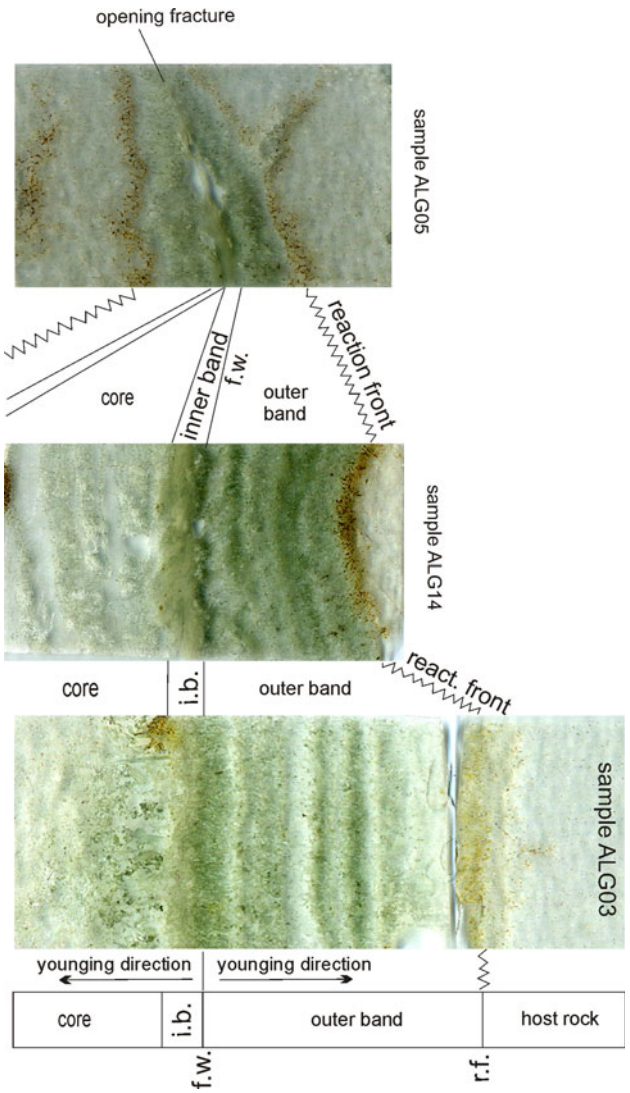

Fig. 3 Schematic structure of a tremolite–calcite vein (according to the model of Bucher 1998). Photographs of thin sections highlight the longitudinal variation of the vein structure. The lowest two thin sections represent one half of the vein. Original height of thin sections is 23 mm. The different microtexture and abundance of tremolite (*green*) and calcite (*colourless*) accounts for the zoned, rhythmic banding of the vein. *r.f.* reaction front, *f.w.* fracture wall, *i.b.* inner band (see text for further explanation)

at 120°. Phlogopite, the only other mineral component of the marble, never exceeds 5% of the rock. Dolomite shows perfect cleavage and twin lamellae, and grains locally contain swarms of fluid inclusions which Micro-Raman analysis revealed to be composed of CO_2, H_2S and COS (Carbonyl sulphide). Intergranular films of Fe–Mn limonitic products are responsible for the brownish colour observed along the vein rims (Figs. 3, 4a).

The veins are mainly composed of tremolite, with lesser amounts of calcite and talc and minor phlogopite and occasional, tiny quartz grains. Veins show very clear rhythmic zoning, produced by alternating layers defined by variations in microstructure and in the mineral proportions of tremolite (+talc) and calcite (Fig. 3).

The outer band consists of a sequence of several layers, each composed of an inner zone rich in tremolite typically forming outwards radiating bundles, and grading into an outer zone where very fine grained (0.2 mm) calcite is prevailing (Fig. 4b). Calcite is interstitial and also included in tremolite. Tremolite is often associated with talc. Modal abundance of tremolite (+talc) and calcite in the whole band is about 7:3 whereas in each layer it ranges from 9:1 to 1:1. Small relic grains of dolomite are also present. In some samples, the layer in contact with the host rock is composed of tremolite, phlogopite and calcite or by thick book-like talc. The inner band consists of very fine grained tremolite (+talc) with minor interstitial calcite. Tremolite forms needles and fibres oriented parallel or at small angle to the axial plane of the vein (Fig. 4c).

The core of the veins is made of very coarse calcite that may include needles and bundles of tremolite (Fig. 4d) and cockades of talc. Cloudy bands within calcite are due to very fine grained swarms of exsolutions of dolomite.

Field and petrographic evidence indicates that these veins formed within massive dolomite marble by reactions with infiltrating fluids along opening fractures. The composition of the reaction products (calcite, tremolite, talc) constrains the infiltrating phase to be a silica-rich aqueous fluid (Bucher 1998) in accordance with reactions:

$$3\underset{(\mathrm{dol})}{CaMg(CO_3)_2} + 4\underset{(\mathrm{qtz_{aq}})}{SiO_{2aq}} + H_2O = 3\underset{(\mathrm{cal})}{CaCO_3} + \underset{(\mathrm{tlc})}{Mg_3Si_4O_{10}(OH)_2} + 3CO_2 \quad (1)$$

and

$$5\underset{(\mathrm{dol})}{CaMg(CO_3)_2} + 8\underset{(\mathrm{qtz_{aq}})}{SiO_{2aq}} + H_2O = 3\underset{(\mathrm{cal})}{CaCO_3} + \underset{(\mathrm{tr})}{Ca_2Mg_5Si_8O_{22}(OH)_2} + 7CO_2 \quad (2)$$

5 Mineral composition

5.1 Analytical methods

Mineral compositions (Tables 1, 2, 3) were analysed by electron microprobe at the CNR-IGG of Padova (Italy), using a Cameca SX50 equipped with four WD spectrometers. Typical measurement conditions were 15 kV acceleration potential, 15 nA beam current, 10 s acquisition time on peak and 5 s on background positions.

The following standards were used: olivine (Mg), ilmenite (Mn, Ti), wollastonite (Ca, Si) corundum (Al), hematite (Fe), orthoclase (K), albite (Na) and fluorite (F). A

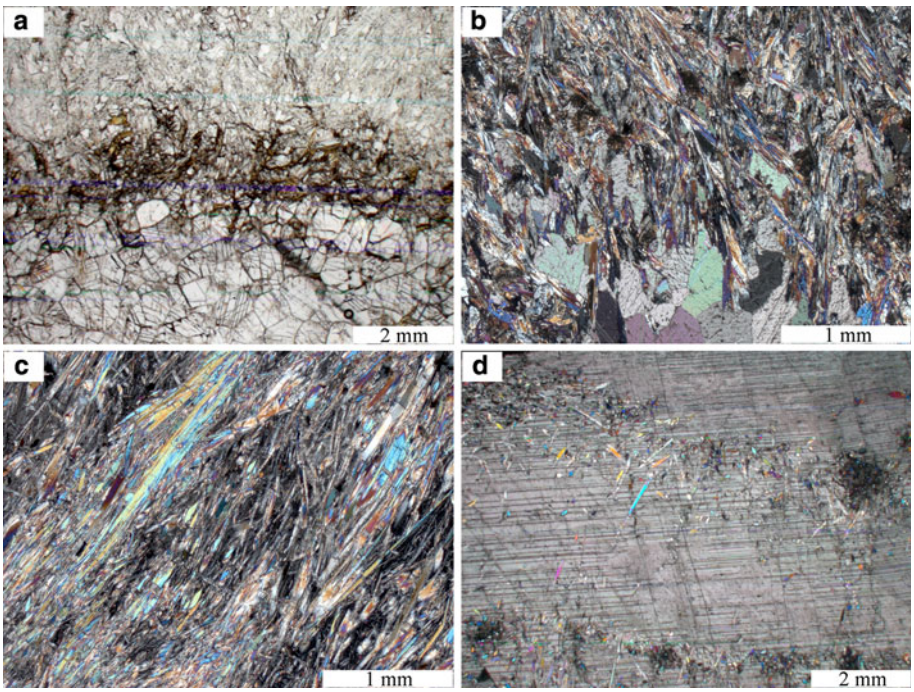

Fig. 4 Representative textures of the tremolite–calcite veins. **a** Outer band, sample ALG14. Reaction front with phlogopite and Fe–Mn oxides between dolomite marble and outward radiating bundles of tremolite with very fine grained calcite. **b** Outer band, sample ALG15, outward radiating bundles of tremolite grading to very fine grained calcite. **c** Inner band, sample ALG02, iso-oriented, fine grained needle- and fibre-like tremolite (+ talc) oriented subparallel to the axial plane. **d** Core, sample ALG14, large, single crystal of spar calcite with needles of tremolite. Thin sections; **a** plane polarised light; **b**, **c**, **d** crossed polars

5 μm sized defocused beam was used during carbonate analysis. The Cameca-PAP program was used to convert x-ray counts into oxide weight percentages. Analyses are accurate to ~2% relative for major and ~5% relative for minor elements.

5.2 Amphibole

Amphibole composition was measured in several veins (Table 1; Fig. 5). Two representative veins, ca. 8–10 cm thick, one from Alagua [ALG3a] and one from Rio Antolina [RAN10] were selected for a detailed investigation of compositional variation of amphibole across the vein. Spot analyses were located at the centre of individual grains, at ca. 100–150 μm step across the vein (Fig. 5). More than 100 analyses were carried out from the contact with the host rock towards the centre of each vein. Because the veins are symmetrical, only one half of the vein was investigated. The calculation of the structural formula was performed using ProbeAmph program (Tindle and Webb 1994). Results were plotted on the amphibole classification diagram following Leake et al. (1997).

At Rio Antolina, amphibole is homogeneous tremolite ($Mg/(Mg + Fe^{2+}) > 0.9$) with only minor actinolite rims (Fig. 5). At Alagua, the composition of amphibole varies from tremolite to Mg-actinolite with $Mg/(Mg + Fe^{2+}) > 0.82$ (Figs. 5, 6). Scanning electron microscope (SEM) imaging during microprobe analysis revealed concentric, oscillatory zoning pattern of amphibole (Fig. 6) not visible under the polarizing microscope, and discordant truncation of zonation surfaces, which possibly reveals the effects of disequilibrium growth with intervening partial dissolution events. To compare the amphibole compositional spread detected across the vein (Fig. 5) with the compositional zoning of individual grains, we carried out 40–60 analyses at close range across selected amphiboles (Fig. 6). The compositional spread observed across the vein overlaps the compositional variation detected in individual zoned amphibole (Figs. 5, 6). No obvious correlation is observed between the compositional variation of amphibole and its modal abundance. A moderate trend of increasing $Mg/(Mg + Fe^{2+})$ content is observed in the coarse-grained calcite-rich core of the vein.

5.3 Talc

Talc has ferroan composition and contains up to 0.5 wt% F in both Alagua and Rio Antolina veins (Table 2). At Rio Antolina, talc close to the contact with the host dolomite has lower FeO content (3.5 wt%) than talc lamellae in the inner part of the vein (4.5 wt%). The iron content in talc, at a given oxygen fugacity (f_{O_2}), depends inversely on temperature (Forbes 1971). The difference in FeO content may thus indicate that talc formed either at slightly different temperatures or under different f_{O_2} conditions.

Table 1 Representative chemical composition of tremolite from Alagua, Rio Antolina and Simbo; the crystallochemical formula is based on 23 atoms of oxygen

	Tremolite												Phlogopite	
	Alagua						Antolina					Simbo	Alagua	Antolina
Analysis	1-Tr1	2-Tr1	3a-Tr1	3a-Tr2	14-Tr1	14-Tr2	5-Tr1	8-Tr1	10-Tr1	10-Tr2	10-Tr3	2-Tr1	14-Ph	10-Ph
SiO_2	58.82	58.58	57.99	58.16	58.24	58.77	59.28	57.77	58.7	58.62	58.12	59.18	41.43	43.48
TiO_2	0.02	0.00	0.01	0.18	0.02	0.02	0.00	0.01	0.02	0.03	0.03	0.02	0.35	0.16
Al_2O_3	0.36	0.53	0.68	1.03	0.95	0.41	0.46	0.24	0.54	0.89	0.59	0.98	13.56	11.9
FeO	3.66	2.46	4.98	2.04	5.88	4.62	1.74	5.2	0.67	1.32	4.52	0.85	8.01	4.38
MnO	0.11	0.22	0.16	0.17	0.25	0.30	0.25	0.38	0.17	0.18	0.40	0.11	0.08	0.07
MgO	21.86	22.68	21.06	23.17	20.67	21.67	23.42	20.9	24.04	23.43	21.32	23.3	21.46	25.00
CaO	13.48	13.45	12.92	13.25	12.89	13.46	13.82	12.86	13.47	13.42	13.06	13.69	0.22	0.20
Na_2O	0.09	0.14	0.17	0.21	0.15	0.11	0.24	0.12	0.18	0.25	0.11	0.07	0.05	0.26
K_2O	0.03	0.06	0.05	0.09	0.06	0.04	0.10	0.05	0.17	0.10	0.05	0.11	9.10	9.00
F	nd	nd	0.09	0.37	0.35	0.30	nd	nd	0.73	0.83	0.32	nd	0.82	2.28
Total	98.43	98.11	98.11	98.67	99.46	99.7	99.29	97.54	98.69	99.07	98.52	98.31	95.06	96.71
Si	8.019	7.985	7.978	7.884	7.943	7.984	7.971	7.998	7.958	7.943	7.976	7.980	5.938	6.015
Al^{iv}	0.000	0.015	0.022	0.116	0.057	0.016	0.029	0.002	0.042	0.057	0.024	0.020	2.062	1.940
Al^{vi}	0.058	0.070	0.088	0.049	0.096	0.050	0.044	0.038	0.044	0.086	0.071	0.137	0.228	0.000
Ti	0.002	0.000	0.001	0.018	0.002	0.002	0.000	0.001	0.002	0.003	0.003	0.002	0.037	0.017
Fe^{3+}	0.000	0.000	0.069	0.111	0.14	0.008	0.000	0.104	0.003	0.00	0.069	0.000	0.000	0.000
Fe^{2+}	0.417	0.280	0.504	0.120	0.531	0.517	0.195	0.499	0.073	0.150	0.450	0.095	0.960	0.506
Mn	0.013	0.025	0.019	0.020	0.029	0.035	0.028	0.045	0.019	0.020	0.047	0.012	0.009	0.008
Mg	4.443	4.608	4.319	4.682	4.203	4.389	4.695	4.314	4.859	4.734	4.360	4.684	4.584	5.155
Ca	1.969	1.965	1.904	1.924	1.884	1.959	1.991	1.908	1.957	1.949	1.920	1.979	0.033	0.029
Na	0.024	0.037	0.045	0.055	0.040	0.029	0.062	0.031	0.048	0.064	0.031	0.017	0.014	0.070
K	0.005	0.010	0.009	0.016	0.010	0.007	0.017	0.01	0.029	0.018	0.009	0.019	1.664	1.588
F	nd	nd	0.039	0.159	0.151	0.129	nd	nd	0.313	0.354	0.139	nd	0.373	0.995
Mg#	0.91	0.94	0.90	0.97	0.89	0.89	0.96	0.90	0.99	0.97	0.91	0.98	0.83	0.91

Average chemical composition of phlogopite from Alagua (mean of two analyses) and Rio Antolina (mean of eight analyses); the crystallochemical formula is based on 22 atoms of oxygen. The standard deviation of the mean values is below 0.5 for major elements, and below 0.2 for minor elements. The database of analyses is available on line as electronic supplementary material (Online Resource 1 & 2)

nd not analysed

Mg# $Mg/(Mg+Fe^{2+})$

5.4 Phlogopite

Phlogopite from Alagua and Rio Antolina show distinct composition in term of MgO (up to 25 wt% in Alagua) and F (up to 2.3 wt%) contents (Table 1).

5.5 Carbonate

Dolomite from Alagua differs from that of Rio Antolina in showing zones with higher iron content (ca. 6 wt% $FeCO_3$). This higher iron content might give reason for the compositional differences observed in amphibole produced from Alagua and Rio Antolina marble. Calcite appears in zones of clear and cloudy appearance, which differ in composition. Microprobe analyses and SEM imaging show that the cloudy appearance results from the presence of tiny dolomite exsolution grains. Calcite from this area contains low, or no, magnesium, whereas calcite from clear areas has up to 3.3 wt% $MgCO_3$ (Table 3).

6 Conditions of tremolite–calcite veins formation

The solubility of Mg in calcite formed in equilibrium with dolomite depends on temperature, and can be used as a geothermometer (Rice 1977; Walther and Helgeson 1980; Powell et al. 1984; Anovitz and Essene 1987). The thermometer provides reliable temperature of calcite formation only when some primary dolomite is left after reaction (Puhan 1995) and magnesian calcite maintains its original composition after formation. The sites for microprobe analysis were therefore carefully selected to avoid cloudy,

Table 2 Average chemical composition of talc from Alagua (sample 3a: 3 analyses; sample 3b: 4 analyses and sample 14: 4 analyses

	Alagua			Antolina	
Analysis	3a-T	3b-T	14-T	8-T1	8-T2
SiO_2	61.83	62.86	63.25	62.8	63.37
Al_2O_3	0.18	0.19	0.33	0.27	0.31
FeO	4.5	3.52	4.42	3.74	3.24
MgO	28.37	29.03	28.6	28.21	29.26
F	0.34	0.36	0.37	nd	nd
Total	95.22	95.97	96.98	95.01	96.17
Si	7.974	8.000	7.997	8056	8012
Al	0.027	0.029	0.049	0.041	0.046
Fe^{2+}	0.486	0.375	0.468	0.401	0.342
Mg	5.456	5.509	5.391	5.395	5.516
F	0.137	0.145	0.149	nd	nd

Standard deviation below 0.9 for SiO_2; 0.6 for MgO and 0.3 for FeO) and representative chemical composition of talc from Rio Antolina; the crystallochemical formula is based on 22 atoms of oxygen. The database of analyses is available on line as electronic supplementary material (Online Resource 3)

nd not analysed

exsolved zones. Several calibrations and empirical equations are reported in literature for the calcite–dolomite geothermometry. Because of the presence of iron (and manganese) in calcite (Table 3), we chose Anovitz and Essene (1987) equation, calibrated in the 400–700°C interval, which takes into account the effect of iron content on the geothermometer. In the present case, the possible effect of manganese in the thermometer can be neglected, because X_{Mn} is <0.03 in the analyzed calcite (Powell et al. 1984). Anovitz and Essene (1987) equation is given for 2 kbar, a pressure that can be assumed comparable with that of formation of the veins (see below). The influence of pressure in the concentration of magnesium in calcite is yet negligible (Goldsmith and Newton 1969), corresponding to a decrease of ca. 5°C per additional kbar (Walther 1983). Results of Walther and Helgeson (1980) and Rice (1977) thermometer are also reported (Table 3), as comparison. The three thermometers provide temperatures consistent with one another (Table 3).

Magnesian-calcite thermometry yields temperature of ~490°C at Alagua and ~450°C at Rio Antolina. Based on petrographic evidence of dolomite exsolution, it is reasonable to assume that 450°C represents the minimum temperature of formation of calcite. The coexistence of talc + calcite + tremolite (+dolomite ± quartz) at a given temperature can be used to calculate the pressure of formation of the assemblage, providing the composition of the coexisting fluid is known (Skippen 1974; Connolly and Tromsdorff 1991; Carmichael 1991; Berman 1991; Puhan 1995). Formation of tremolite (and talc) by reaction (2) [and (1)] consumes H_2O and liberates CO_2, driving the initial fluid composition to higher X_{CO_2} values. Assuming a reasonable range of fluid composition (X_{CO_2} between 0.2 and 0.5) in a pure CaO–MgO–SiO_2–H_2O–CO_2 system (Berman 1988), we estimate that veins formed at a minimum *P* of 2–3 kbar (Fig. 7).

7 Tremolite–calcite veins formation mechanism

The tremolite–calcite veins that crosscut the dolomite marble of the Baceno and Tèggiolo metasediments occur in a geological and structural setting that is similar to that of veins in Campolungo (Mercolli et al. 1987). However their mechanism of formation differs significantly. Unlike in Campolungo, the tremolite–calcite veins we describe did

Table 3 Representative chemical composition of carbonates from Alagua and Rio Antolina

	Calcite				Dolomite			
	Alagua		Antolina		Alagua		Antolina	
Analysis	14-C1	3a-C1	10-C1	10-C2	14-D1	14-D2	10-D1	10-D2
$MgCO_3$	3.32	2.96	2.68	2.69	45.07	36.24	36.85	44.46
$CaCO_3$	95.03	95.78	95.68	96.31	54.07	54.94	60.95	55.16
$MnCO_3$	0.84	0.88	0.56	0.7	0.12	1.81	1.02	0.02
$FeCO_3$	0.89	0.81	0.28	0.42	0.12	6.11	1.49	0.00
Total	100.08	100.43	99.2	100.11	99.38	99.11	100.3	99.64
X_{Mg}	0.039	0.035	0.032	0.032	0.496	0.41	0.409	0.489
X_{Ca}	0.946	0.95	0.961	0.959	0.502	0.524	0.57	0.511
X_{Fe}	0.008	0.007	0.002	0.004	0.001	0.05	0.012	0.000
X_{Mn}	0.007	0.008	0.005	0.006	0.001	0.015	0.008	0.000
(1) *T* (°C)	491	469	445	447				
(2) *T* (°C)	480	459	443	442				
(3) *T* (°C)	497	479	465	466				

Temperature calculation after (1) Anovitz and Essene (1987); (2) Walther and Helgeson (1980) and (3) Rice (1977) equations. The database of analyses is available on line as electronic supplementary material (Online Resource 4)

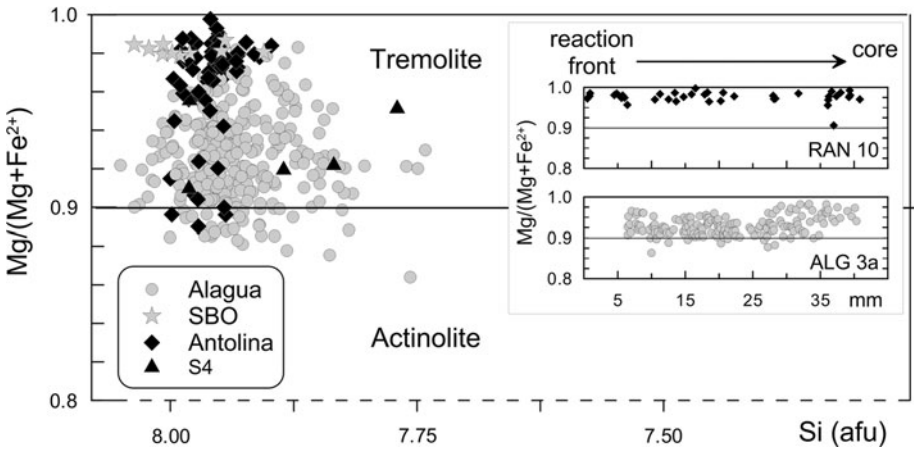

Fig. 5 $Mg/(Mg+Fe^{2+})$ versus Si (*afu* atoms per formula unit) amphibole classification diagram (after Leake et al. 1997). All samples have $(Na+K)_A < 0.50$ and $Ti < 0.50$. Only the relevant part of the actinolite field $(Mg/(Mg+Fe^{2+}) > 0.8$ is reported. The inset illustrates the compositional variation of amphibole from the reaction front to the core, across two representative thin sections ca. 40 mm large

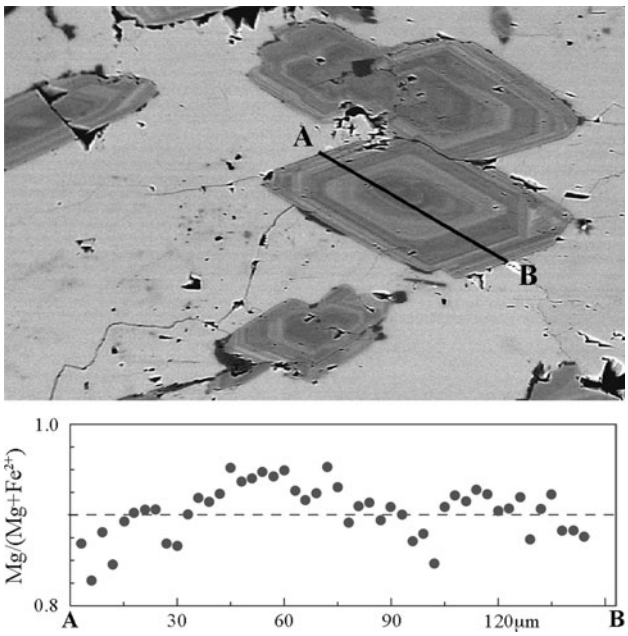

Fig. 6 Sample ALG03a. BSE imaging reveals concentric, oscillatory zoning pattern of amphibole. The pattern of $Mg/(Mg+Fe^{2+})$ along the *black line* A–B drawn across the amphibole is shown

not form by reaction with preexisting quartz and dolomite marble with fluids of very high salinity.

Bucher-Nurminen (1981, 1989) and Bucher (1998) made a detailed investigation on the formation of tremolite and the growth mechanism of tremolite–calcite veins in dolomite rafts inside the Bergell granite. The texture and composition of simple veins (as well as the host rock) described by Bucher-Nurminen (1989) are strikingly similar to those described in this work, and we claim that the formation mechanism was also comparable. In both cases tremolite and calcite developed as a product of the reaction (2) between a silica-rich aqueous fluid and the dolomite marble. This reaction produces 71 vol% tremolite and 29 vol% calcite similar to the overall modal abundances estimated in Alagua and Rio Antolina veins. In Fig. 3 we sketch the structure of a representative vein from Alagua and we summarize the main features of the growing mechanism following the fracture-reaction model proposed by Bucher-Nurminen (1989). According to this model, the central part or inner band of the veins thickened by deposition of material in an opening fracture, whereas the external part or outer band of the veins, between the former vein wall and the reaction front, grew by replacement of dolomite with products of reactions (1) and (2).

The brownish rim at the contact with the host dolomite marks the boundary of the reaction front.

The rhythmic sequence of tremolite + calcite bands (clearly seen in ALG14 and ALG03 thin sections) represents the zone of replacement of dolomite by reaction (2), as proven by remnants of dolomite around newly formed tremolite prism and interstitial patches of dolomite amid tremolite aggregates, as observed at SEM imaging. In these bands, the typical texture of tremolite aggregates, radiating outwards normal to the fracture wall, is explained with the volume increase of about 19% associated with reaction (2) which would favoured the growth of tremolite needles in this direction (Bucher 1998). Rosette-like or bundles of tremolite aggregates suggest a high reaction rate in the presence of H_2O-rich fluid (Puhan 1995). The rhythmic sequence of tremolite + calcite bands observed at Alagua and Rio Antolina can be produced by changes in silica activity $(a_{SiO_2(aq)})$ and X_{CO_2} due to pressure variations during cyclical stages of stress build-up and stress-drop (Bucher-Nurminen 1989). This mechanism modifies the solubility of calcite and hence the modal calcite/tremolite ratio in the replacement zone. Oscillatory chemical zoning and petrographic evidence of dissolution and precipitation recorded by tremolite represent non-equilibrium features consistent with repeated episodes of pressure variation. The restricted chemical variation of tremolite across the veins (Fig. 5) testifies for a nearly constant composition of the infiltrating fluid (Bucher-Nurminen 1989).

At the inner band of the vein (Fig. 4c), tremolite (+talc) arranged parallel to the vein formed by deposition along the fracture wall. Precipitation of coarse-grained calcite

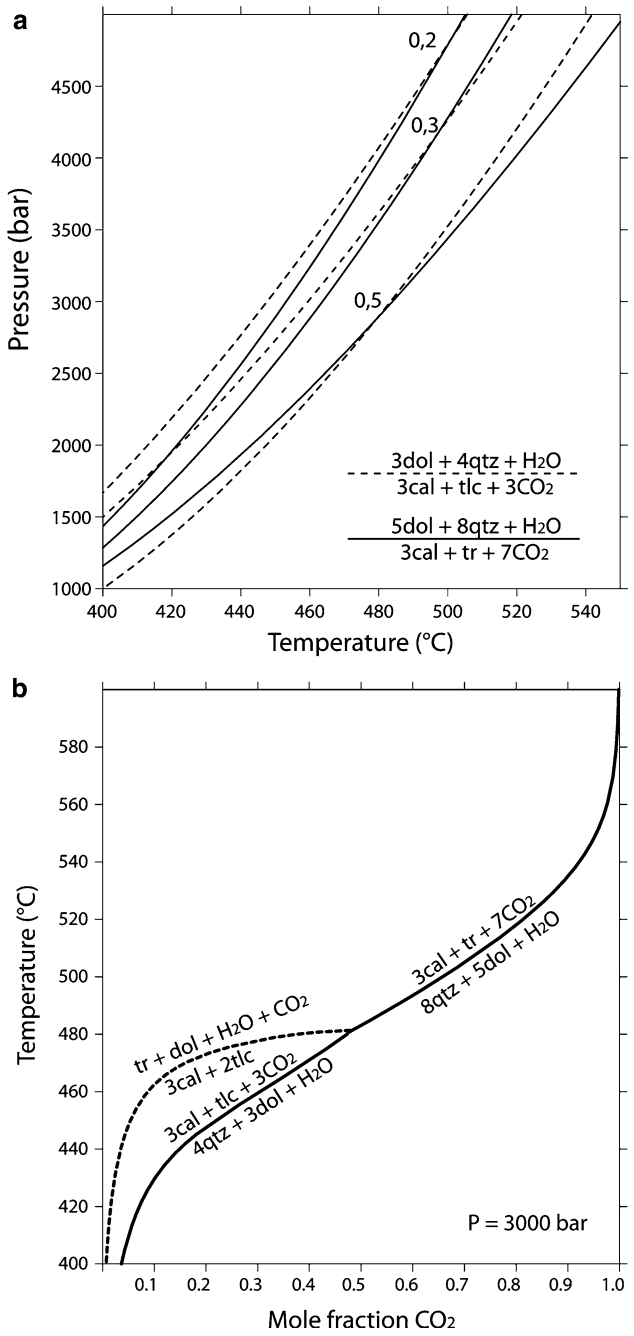

Fig. 7 P–T phase (**a**) and T–X_{CO_2} (**b**) diagrams for the indicated reactions. $P_{CO_2} + P_{H_2O} = P_{tot}$. **a**: X_{CO_2} values are labelled on each couple of curves. Plotted with winTWQ (version 2.32) software (Berman 1991) and relevant database

(with minor tremolite) in the central part of the fracture eventually sealed the vein.

8 Discussion and conclusions

The tremolite–calcite veins from the Antigorio Valley formed in dolomite marble by infiltration of a silica-rich fluid at temperature of 450–490°C and minimum pressure of about 2–3 kbar. The veins developed along fractures, are undeformed and clearly post-date the regional ductile deformation.

Tremolite–calcite veins occur over a wide area within the metasedimentary units at both the top (Alagua and Simbo) and the bottom (Rio Antolina and boreholes) of the Antigorio nappe. Significant silica-rich fluid influx must therefore have affected the entire rock volume of this region in the core of the Verampio window, in the footwall of the Simplon Fault. This is also testified by the presence, in the same region, of abundant quartz-veins in gneiss of the Antigorio and Monte Leone nappes. It is likely that at least some of these quartz-veins derived from infiltration of same silica rich fluids that originated the tremolite–calcite veins. Some of the quartz-veins are dated and might have potential in constraining the age of formation of the tremolite–calcite veins.

Wawrzyniec et al. (1999) studied both aqueous and mixed H_2O–CO_2 fluid inclusions from quartz veins in the immediate footwall of the Simplon Fault and estimated that entrapment conditions for all fluid inclusions were >500°C and >5 kbar. These veins indicate that fracturing was already active at PT conditions higher than those in which the tremolite–calcite veins formed.

Silica-rich fluids precipitated also in brittle- or semi-brittle structure such as quartz fillings in undeformed necks of foliation boudinages frequently visible in the Antigorio and Monte Leone gneiss. Similar brittle quartz–muscovite–calcite veins in necks of foliation boudinage in Monte Leone gneiss were recently dated by Campani et al. (2010a, b) at ~14.5 Ma, an age they interpret as the time of transition from ductile to brittle behaviour in mylonites of the Simplon Fault. K/Ar ages of 14–11 Ma for biotite, muscovite and adularia growing as undeformed fissure minerals in quartz veins from the Simplon region (Purdy and Stalder 1973) are consistent with quartz-vein formation and brittle fracturing at around 14–15 Ma. Undeformed gold–quartz veins emplaced at 11.6 Ma at the Gondo Filone Maffiola and at 10.6 Ma at the Crodo Alfenza mine ($^{40}Ar/^{39}Ar$ on muscovite) formed at temperatures between 300 and 350°C (Pettke et al. 1999, 2000) namely at cooler conditions, and later, than the tremolite–calcite veins considered here.

Tremolite–calcite veins appear to have developed relatively late in the tectonic history, possibly at the same time of quartz veins during cooling and exhumation in the footwall of the low-angle normal Simplon Fault. Cooling and exhumation history of this area was modelled by Grasemann and Mancktelow (1993) and more recently by Campani et al. (2010b). One of the geochronological samples (D) used by Grasemann and Mancktelow (1993) to compare their numerical thermal modelling of exhumation,

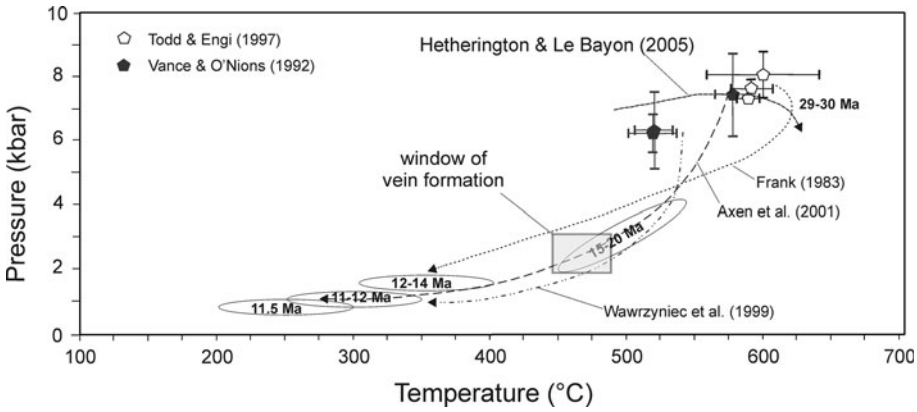

Fig. 8 Window of the PT conditions of vein formation drawn on the PT exhumation paths for the Simplon dome compiled from the quoted authors

approximately corresponds to the position in the footwall of the tremolite–calcite veins of Rio Antolina and, according to their thermal model F2, this sample cooled through 450°C around 15 Ma.

From the cooling curves of Grasemann and Mancktelow (1993) and the direct dating of the regional brittle-ductile transition in several quartz-rich veins (Campani et al. 2010a, b), we infer that tremolite–calcite veins also formed around 14–15 Ma.

The exhumation of the Simplon footwall has been reconstructed by many authors also by means of T–t and P–T paths (Frank 1983; Vance and O'Nions 1992; Todd and Engi 1997; Wawrzyniec et al. 1999; Axen et al. 2001; Hetherington and Le Bayon 2005). Tremolite–calcite veins have a PT window for their formation between 450–490°C and 2–3 kbar. Plotting these data on a diagram compiled from the published PT paths for the Simplon dome (Fig. 8), they fit well with the exhumation path proposed by Axen et al. (2001).

During the exhumation of the footwall of the Simplon Fault, 14–15 Ma ago, the nappe pile crossed the transition to dominant brittle behaviour promoting the development of fracture networks that crossed the entire nappe stack leading to the formation of quartz veins in the gneiss and tremolite–calcite veins in the dolomite marbles.

Given the mechanism of formation of tremolite–calcite veins and the fracturing of the region during exhumation, it is expected that veins similar to those described in this paper are more widespread than so far reported in literature in dolomite marble within the whole Mesozoic metasedimentary sequences of Baceno and Tèggiolo. This is corroborated by evidence for vein occurrences as retrieved from boreholes.

Acknowledgments The authors are indebted to Neil Mancktelow who greatly improved the manuscript. We thank T. Burri and M. Engi for detailed and constructive reviews. We thank D. Pedron for Raman analyses and R. Carampin for technical support during EMP analyses. We thank also E. Gnos for editorial handling.

References

Anovitz, L. M., & Essene, E. J. (1987). Phase equilibria in the system CaCO3–MgCO3–FeCO3. *Journal of Petrology, 28*, 389–415.

Axen, G. J., Selverstone, J., & Wawrzyniec, T. (2001). High-temperature embrittlement of extensional Alpine mylonite zones in the midcrustal ductile-brittle transition. *Journal of Geophysical Research, 106*(B3), 4337–4348.

Berman, R. G. (1988). Internally-consistent thermodynamic data for minerals in the system Na_2O–K_2O-CaO-MgO-FeO-Fe_2O_3-Al_2O_3-SiO_2-TiO_2–H_2O-CO_2. *Journal of Petrology, 29*, 445–522.

Berman, R. G. (1991). Thermobarometry using multi-equilibrium calculations: a new technique, with petrological applications. *Canadian Mineralogist, 29*, 833–855.

Bianconi, F. (1971). Geologia e petrografia della regione del Campolungo. Beiträge zur Geologischen Karte der Schweiz, 142.

Bucher, K. (1998). Growth mechanism of metasomatic reaction veins in dolomite marbles from Bergell Alps. *Mineralogy and Petrology, 65*, 151–171.

Bucher-Nurminen, K. (1981). The formation of metasomatic reaction veins in dolomitic marble roof pendants in the Bergell intrusion (Province Sondrio, Northern Italy). *American Journal of Science, 281*, 1197–1222.

Bucher-Nurminen, K. (1989). Reaction veins in marble formed by a fracture-reaction-seal mechanism. *European Journal of Mineralogy, 1*, 701–714.

Campani, M., Mancktelow, N., Seward, D., Rolland, Y., Müller, W., & Guerra, I. (2010a). Geochronological evidence for continuous exhumation through the ductile-brittle transition along a crustal-scale low-angle normal fault (Simplon Fault Zone, Central Alps). *Tectonics*, *29*, TC3002, doi:10.1029/2009TC002582.

Campani, M., Herman, F., & Mancktelow, N. (2010b). Two- and three-dimensional thermal modelling of a low-angle detachment: Exhumation history of the Simplon Fault Zone, central Alps. *Journal of Geophysical Research, 115*, B10420. doi:10.1029/2009JB007036.

Carmichael, D. M. (1991). Univariant mixed-volatile reactions: Pressure-temperature phase diagrams and reaction isograds. *Canadian Mineralogist, 29*, 741–754.

Castiglioni, G. (1958). Studio geologico e morfologico del territorio di Baceno e Premia (Val d'Ossola–Alpi Lepontine). *Memorie degli Istituti di Geologia e Mineralogia dell'Università di Padova*, *XX*, 2–82.

Cinque, F. (1939). Il « Marmo di Crevola » ed i suoi minerali. *Atti Società Italiana Scienze Naturali*, *78*, 202–223.

Connolly, J. A. D., & Tromsdorff, V. (1991). Petrogenetic grid for metacarbonate rocks: Pressure-temperature phase-diagram projection for mixed-volatile systems. *Contributions to Mineralogy and Petrology, 108*, 93–105.

Escher, A., Masson, H., & Steck, A. (1993). Nappe geometry in the Western Swiss Alps. *Journal of Structural Geology, 15*, 501–509.

Forbes, W. C. (1971). Iron content of talc in the system Mg3Si4O10(OH)2–Fe3Si4O10(OH)2. *Journal of Geology, 79*, 63–74.

Frank, E. (1983). Alpine metamorphism of calcareous rocks along a cross-section in the Central Alps: Occurrence and breakdown of muscovite, margarite and paragonite. *Schweizerische Mineralogische und Petrographische Mitteilungen, 63*, 37–93.

Goldsmith, J. R., & Newton, R. C. (1969). P-T-X relations in the system $CaCO_3$–$MgCO_3$ at high temperatures and pressures. *American Journal of Science, 267A*, 160–190.

Grasemann, B., & Mancktelow, N. (1993). Two-dimensional thermal modelling of normal faulting: The Simplon Fault Zone, Central Alps, Switzerland. *Tectonophysics, 225*, 155–165.

Herwegh, M., & Pfiffner, O.A. (1999). Die Gesteine der Piora-Zone (Gotthard Basistunnel). In: Löw, S. & Wyss, R. (Eds.): Vorerkundung und Prognose der Basistunnels am Gotthard und am Lötschberg. Balkema, Rotterdam, 77–88.

Hetherington, C. J., & Le Bayon, R. (2005). Bulk rock composition: a key to identifying invisible prograde reactions in zoned garnet. *Schweizerische Mineralogische und Petrographische Mitteilungen, 85*, 57–67.

Keller, L. M., Hess, M., Fügenschuh, B., & Schmid, S. (2005). Structural and metamorphic evolution of the Camughera–Moncucco, Antrona and Monte Rosa units southwest of the Simplon line, Western Alps. *Eclogae Geologicae Helvetiae, 98*, 19–49.

Kuhn, B. K., Reusser, E., Powell, R., & Günther, D. (2005). Metamorphic evolution of calc- schists in the Central Alps, Switzerland. *Schweizerische Mineralogische und Petrographische Mitteilungen, 85*, 175–190.

Leake, B. E., Woolley, A. R., Birch, W. D., Burke, E. A. J., Ferraris, G., Grice, J. D., et al. (1997). Nomenclature of amphiboles: report of the subcommittee on amphiboles of the International Mineralogical Association, commission on new minerals and mineral names. *The Canadian Mineralogist, 35*, 219–246.

Leu, W. (1986). Lithostratigraphie und Tektonik der nordpenninischen Sedimente in der Region Bedretto-Baceno-Visp. *Eclogae Geologicae Helvetiae, 79*, 769–824.

Mancktelow, N. S. (1985). The Simplon line: A major displacement zone in the western Lepontine Alps. *Eclogae Geologicae Helvetiae, 78*, 73–96.

Maxelon, M., & Mancktelow, N. S. (2005). Three-dimensional geometry and tectonostratigraphy of the Pennine zone, Central Alps, Switzerland and Northern Italy. *Earth-Science Reviews, 71*, 171–227.

Mercolli, I., Skippen, G., & Trommsdorff, V. (1987). The tremolite veins of Campolungo and their genesis. *Schweizerische Mineralogische und Petrographische Mitteilungen, 67*, 75–84.

Pettke, T., Diamond, L. W., & Kramers, J. D. (2000). Mesothermal gold lodes in the north- western Alps: A review of genetic constraints from radiogenic isotopes. *European Journal of Mineralogy, 12*, 213–230.

Pettke, T., Diamond, L. W., & Villa, I. M. (1999). Mesothermal gold veins and metamorphic devolatilization in the northwestern Alps: The temporal link. *Geology, 27*(7), 641–644.

Pini, E. (1786). Osservazioni sui feldspati ed altri fossili singolari dell'Italia. *Memorie di Matematica e Fisica della Società Italiana di Scienze Naturali, 3*, 688–717.

Powell, R., Condliffe, D. M., & Condliffe, E. (1984). Calcite–dolomite geothermometry in the system $CaCO_3$-$MgCO_3$-$FeCO_3$: an experimental study. *Journal of Metamorphic Geology, 2*, 33–41.

Puhan, D. (1995). Metamorphic evolution of the assemblage tremolite + talc + calcite + dolomite + quartz within a sample of siliceous dolomite from the southern Damara Orogen (Namibia). *Contribution to Mineralogy and Petrology, 120*, 180–185.

Purdy, J. W., & Stalder, H. A. (1973). K-Ar ages of fissure minerals from the Swiss Alps. *Schweizerische Mineralogische und Petrographische Mitteilungen, 53*, 79–98.

Rice, J. M. (1977). Progressive metamorphism of impure dolomitic limestone in the Marysville aureole, Montana. *American Journal of Science, 277*, 1–24.

Schardt, H. (1903). Note sur le profil géologique et la tectonique du massif du Simplon comparées aux travaux antérieurs. *Eclogae Geologicae Helvetiae, 8*, 173–200.

Schmidt, C., & Preiswerk, H. (1905). Geologische Karte der Simplongruppe. Beiträge zur Geologischen Karte der Schweiz, [N.F.] 26, Spezialkarte No. 48.

Skippen, G. B. (1974). An experimental model for low pressure metamorphism of siliceous dolomitic marble. *American Journal of Science, 274*, 487–509.

Steck, A. (2008). Tectonics of the Simplon massif and Lepontine gneiss dome: deformation structures due to collision between the underthrusting European plate and the Adriatic indenter. *Swiss Journal of Geoscience, 101*, 515–546.

Steck, A., Bigioggero, B., Dal Piaz, G.V., Escher, A., Martinotti, G., & Masson, H. (1999). Carte géologique des Alpes de Suisse occidentale, 1:100000, Carte géologique spéciale N°123. Service Hydrologique et Géologique National (Berne).

Tindle, A. G., & Webb, P. C. (1994). Probe-Amph: A spreadsheet program to classify microprobe-derived amphibole analyses. *Computers and Geosciences, 20*, 1201–1228.

Todd, C. S., & Engi, M. (1997). Metamorphic field gradients in the Central Alps. *Journal of Metamorphic Geology, 15*, 513–530.

Trommsdorff, V. (1966). Progressive Metamorphose kieseliger Karbonatgesteine in den Zentralalpen zwischen Bernina und Simplon. *Schweizerische Mineralogische und Petrographische Mitteilungen, 46*, 431–460.

Trommsdorff, V., & Skippen, G. (1986). Vapour loss ("Boiling") as a mechanism for fluid evolution in metamorphic rocks. *Contribution to Mineralogy and Petrology, 94*, 317–322.

Vance, D., & O'Nions, R. K. (1992). Prograde and retrograde thermal histories from the Central Swiss Alps. *Earth and Planetary Science Letters, 114*, 113–129.

Walther, J. V. (1983). Description and interpretation of metasomatic phase relations at high pressures and temperatures: 2 Metasomatic reactions between quartz and dolomite at Campolungo, Switzerland. *American Journal of Science, 283A*, 459–485.

Walther, J. V., & Helgeson, H. C. (1980). Description and interpretation of metasomatic phase relations at high pressures and temperatures: 1. Equilibrium activities of ionic species in nonideal mixtures of CO_2 and H_2O. *American Journal of Science, 280*, 575–606.

Wawrzyniec, T., Selverstone, J., & Axen, G. J. (1999). Correlations between fluid composition and deep-seated structural style in the footwall of the Simplon low-angle normal fault, Switzerland. *Geology, 27*, 715–718.

Zwingmann, H., & Mancktelow, N. (2004). Timing of Alpine fault gauges. *Earth and Planetary Science Letters, 223*, 415–425.